

$$^{14}\text{N}(p,\gamma)^{15}\text{O}$$

A Dissertation

Submitted to the Graduate School  
of the University of Notre Dame  
in Partial Fulfillment of the Requirements  
for the Degree of

Doctor of Philosophy

by  
Bryce Alan Frentz

---

Ani Aprahamian, Director

Graduate Program in Physics

Notre Dame, Indiana

November 2019

$$^{14}\text{N}(p,\gamma)^{15}\text{O}$$

Abstract

by

Bryce Alan Frentz

$$^{14}\text{N}(p,\gamma)^{15}\text{O}$$

What do you even put in an abstract for a thesis? Seems a little ridiculous...

Bananas is fruits. Tacos is sandwiches.

NEW DEDICATION NAME

To .... probably nobody

## CONTENTS

Figures . . . . .	v
Tables . . . . .	vi
Preface . . . . .	vii
Acknowledgments . . . . .	viii
Symbols . . . . .	ix
Features of Formatting in This Example File . . . . .	1
Chapter 1: Introduction . . . . .	2
1.1 Overview . . . . .	2
1.1.1 General overview . . . . .	2
1.1.2 Stellar evolution . . . . .	3
1.1.3 Hydrogen Burning . . . . .	4
1.2 Thermonuclear reaction rates . . . . .	7
1.3 Nuclear reactions . . . . .	12
1.3.1 Direct capture reactions . . . . .	12
1.3.2 Resonant reactions . . . . .	13
1.4 R-matrix theory . . . . .	15
1.5 The $^{14}\text{N}(p, \gamma)^{15}\text{O}$ reaction . . . . .	17
1.5.1 Reaction cross-section . . . . .	17
1.5.2 Lifetime . . . . .	17
1.6 The Doppler Shift Attenuation Method for lifetime measurements . . . . .	17
1.7 Thesis outline . . . . .	17
Chapter 2: Experimental setup and procedures . . . . .	19
2.1 Introduction . . . . .	19
2.2 Accelerators, beamline, and high-purity Germanium detectors . . . . .	19
2.2.1 Van de Graaff accelerators . . . . .	19
2.2.2 Ion sources . . . . .	19
2.2.3 Beamline . . . . .	19
2.3 High-purity Germanium detectors . . . . .	19
2.4 Cross-section measurements . . . . .	19
2.5 Lifetime measurement . . . . .	19
Chapter 3: Cross section data Reduction and analysis . . . . .	20
3.1 Introduction . . . . .	20
3.2 Energy calibration . . . . .	20
3.3 Efficiency . . . . .	20
3.3.1 Total efficiency . . . . .	20

3.3.2	Full energy peak efficiency . . . . .	20
3.4	Summing corrections . . . . .	20
3.5	Target characterization . . . . .	20
3.6	Cross-section determination . . . . .	20
Chapter 4:	Monte Carlo simulations for lifetime measurements with DSAM . . . . .	21
4.1	Simulations with the Geant4 package . . . . .	21
4.2	Determining a nuclear lifetime . . . . .	21
Chapter 5:	The lifetime of the 6.79 MeV state in $^{15}\text{O}$ . . . . .	22
5.1	Data analysis . . . . .	22
5.1.1	Lifetime of <b>ANOTHER STATE, 6.17 MeV maybe</b> . . . . .	22
5.1.2	Lifetime of the 6.79 MeV state in $^{15}\text{O}$ . . . . .	22
Chapter 6:	R-matrix analysis . . . . .	23
6.1	Fits to the capture data . . . . .	23
6.2	Inclusion of the new lifetime . . . . .	23
Chapter 7:	Results and conclusions . . . . .	24
Appendix A:	GNU GENERALISMS . . . . .	25
A.1	Definitions . . . . .	25
Bibliography	. . . . .	29

## FIGURES

1.1	Schematic plot of the combined attractive nuclear and repulsive Coulomb potentials.	9
1.2	The energy dependence of the nuclear cross section and astrophysical S-factor . . .	10
1.3	The two dominant terms of the reaction rate calculation and their convolution (Gamow peak). . . . .	11
1.4	An energy level diagram of the $^{14}\text{N}(p,\gamma)^{15}\text{O}$ reaction. This shows the pathways of decay to the ground state of the $^{15}\text{O}$ nucleus. The paths shown in red indicate a resonance reaction, with the formation of the compound nucleus in an excited state, while the path in blue shows a direct capture process, proceeding immediately to the ground state. . . . .	12

## TABLES

A.1	Commonly used Gnu Terms . . . . .	26
A.2	Top Ten Gnus From Table ?? With Reviewer Comments. Gnus are Listed Below in Alphabetic Order. . . . .	28

## PREFACE

It is often said that there are few places left to be discovered or explored. That's only true on the human scale. Using a magnifying glass, microscope, telescope or any other number of devices allows us to transcend our scale.

Taken in isolation, different structures are like characters in a story. Each contributes something to the overall shape. Sometimes one or a handful of characters will dominate the story, but it is only when put together that they fully explain why the world behaves the way it does.

The stars twinkle their cryptic morse code and nuclear physics is one of the best keys to their cypher.

When numbers acquire the significance of language they acquire the power to do all of the things that language can do. Describe power history success failure victory defeat character grace to become fiction, drama, and poetry.

Discovering stable relationships in a seemingly unstable world.



## ACKNOWLEDGMENTS

I would like to acknowledge ...

## SYMBOLS

$\mathcal{F}$	sighting frequency of Gnus about campus
$p$	student population
$f$	type of food available
$d$	day of week
$c$	speed of light
$m$	mass
$e$	elementary charge
$a, b$	miscellaneous constants
$E$	energy

## FEATURES OF FORMATTING IN THIS EXAMPLE FILE

This **chapter** has been added to the original sample file to highlight the various features with the formatting that conforms to the Graduate school guidelines — whether obtained due to the use of `NDdiss2 $\epsilon$`  class file or just plain good practice.

- An important note on line-breaks via `\` in titles: the titles of the thesis as well as chapters and table captions use `\MakeTextUppercase{}` from the `textcase` package. Due to the nature of the `center` environment, any line-breaks introduced in titles and captions should be protected, as in `\protect\`. To preserve the case in titles and captions, use, e.g., `\NoCaseChange{Gnus}`.
- In the *dedication*, the title name has been modified. So, you know how to and that it can be done.
- The entries in the *List of figures* and *List of Tables* are single-spaced themselves but are double-spaced from the other.
- The table captions are not in all CAPS as well for the reason mentioned above.
- Appropriate space is left between the `Table xx` and its corresponding caption (which is double-spaced itself) as in table `??`.
- Tables look much better without the vertical lines (good practice).
- There is double-spacing between the table entries but single-spacing within the entry.
- The chapter (see Chapter `??`) or section titles are double-spaced as mentioned in the guidelines.
- There is a `subsubsection` present (eg. section `??`) and is properly formatted in the TOC.
- Sections deeper than `subsubsection` should not appear in the TOC.
- Table A.1 is an example of the use of `landscape` environment in which a normal table is formatted in a *landscape* mode.
- The `longtable` environment is used in Tables `??` and A.2, in normal and `landscape` mode, respectively. The table captions are formatted properly in both cases.
- In the table `??`, the `footnote` in the table header does not appear at all. This is not an error of the `NDdiss2 $\epsilon$`  class but of the `longtable` package.
- An example of citing a website is shown in the bibliography (see `[? ]`) which is formatted using the `nddiss2e.bst` citation style file.
- A bit of information on the `NDdiss2 $\epsilon$`  class file and the typesetting program used is included in a box on the last page of the thesis.
- Footnotes should space properly.
- Items in `itemize`, `enumerate`, and `description` environment should automatically single-space within an item, but double space between items.

## CHAPTER 1

## INTRODUCTION

## 1.1 Overview

## 1.1.1 General overview

Nuclear physics data, in both the forms of theoretical predictions and experimental results, is an ever richer trove of information useful in solving many astrophysical problems. The partnership between the fields of nuclear physics and astrophysics was actually born in the early days of nuclear physics when Sir Arthur Eddington postulated that recent laboratory discoveries could explain the energy generation of the sun and stars [citeIliadisBook](#). Therefore, developments in one area naturally link to increased knowledge in the other - a scientific point and counterpoint. It follows naturally that many astrophysical phenomena are governed by nuclear physics. So it is through this study of the microscopic aspects of the universe that we also elucidate its behavior in the grandest scales imaginable.

The general goals of the field of nuclear astrophysics are as follows:

- to understand the processes by which the chemical elements were formed
- to understand the mechanism(s) responsible for the the relative abundances between the chemical elements
- to understand the energy generation during each phase of stellar evolution.

Crucially, stellar evolution is cyclic: stars are born, evolve, and ultimately die, seeding the interstellar medium with the collective material they've created over their life in order to form the building blocks for the next stellar generation. As each of the different stellar phases are guided by the underlying nuclear physics, investigations into these questions provide a rich ink between humans and our place in the cosmos.

The synthesis of the chemical elements we see began with the universe as the Big Bang created hydrogen, helium, and trace amounts of lithium [citeAlpher1948](#). Shortly after the Big Bang, the temperature and density of the Universe dropped too low for any significant nuclear fusion to occur and overcome the mass 5 and mass 8 barriers. This was the end of Big Bang Nucleosynthesis (BBN),

as after this point, the elemental abundances were nearly stable, with the only changes coming from the radioactive decay of  ${}^3\text{He} \rightarrow t$  and  ${}^7\text{Be} \rightarrow {}^7\text{Li}$  citeFields2011.

From this point, generations of stellar evolution created nearly all other elements, leading to the currently observed elemental abundance distribution, shown in Figure ?? . The synthesis of elements heavier than BBN products, commonly referred to as "metals," began with the formation of the first stars. Cold gas clouds, composed primarily the BBN products of hydrogen and helium (and metals in subsequent stellar generations), coalesce under their mutual gravitational attraction, converting their gravitational potential energy to heat – increasing their pressure, density, and temperature. Upon passing a critical threshold for these physical quantities, typically temperatures  $>1$  MK, thermonuclear fusion reactions begin in the core citeRyanNortonBook. This transition marks the "birth" of a star, having reached a point where nuclear reactions provide a sufficient heat source to balance energy losses from radiation.

### 1.1.2 Stellar evolution

Every star is unique and their intrinsic quantities when forming, such as mass or initial abundance distribution, prescribe the nuclear reactions that can occur throughout their lifetimes. Despite their differences, correlations emerge in studies of their observational properties , like luminosity, mass distribution, temperature, color, etc. The most evident patterns appeared when classifying stars by luminosity (or magnitude) vs temperature (or color), named the *Hertzsprung-Russel* (HR) diagram citeCarrollOstlieBook, IliadisBook, RyanNortonBook, distilling the most important relationship between stellar properties. An example HR diagram for stars in the solar neighborhood is displayed in Figure ?? . Since HR diagrams represent a snapshot of the evolutionary tack of a set of stars, the most densely populated areas of such plots are those in which individual stars necessarily spend most of their lives. Conversely, as there is a lower probability of observing a star in a short-lived phase, sparsely populated areas of HR diagrams detail such phases of stellar burning.

The vast majority of stars lie on the diagonal band stretching from the upper left (hot, bright stars) to the lower right (cool, faint stars) of the diagram. This feature is called the main sequence. These stars support themselves through core hydrogen burning – implying that stars spend most of their lives in this long period of quiescent hydrogen burning in the *pp chains* and the CNO cycles, detailed in subsequent sections. Other prominent features of typical HR diagrams are the clusters of stars in the upper quadrants (very bright stars), commonly referred to as the giant branch, the lower

left quadrant (hot, faint stars), where the white dwarf stars reside, and the lower right quadrant beyond the main sequence, occupied by brown dwarfs. Each classification corresponds to different nuclear reactions, with stars evolving off the main sequence being characterized by phases of burning of heavier elements, like helium or carbon.

Any single star's evolutionary track will follow different paths depending on its initial mass [citeIliadisBook](#), [RyanNortonBook](#). For cosmic objects of mass  $\lesssim 0.08 M_{\odot}$ , where  $M_{\odot}$  is the mass of the sun, core temperatures never rise high enough to sustain hydrogen fusion, and thus they evolve directly into brown dwarf stars. In the range of mass  $0.08 M_{\odot} \lesssim M \lesssim 0.4 M_{\odot}$ , stars undergo core hydrogen fusion through the *pp chains*, but do not reach temperatures sufficient to initiate helium burning after exhausting hydrogen in the core. Ultimately, stars in this classification become white dwarfs. The next mass grouping consists of Sun-like stars, with masses  $0.4 M_{\odot} \lesssim M \lesssim 8.0 M_{\odot}$ , which evolve off the main sequence and continue growing and burning (both in the stellar core and shells in their stellar envelope). Such stars achieve temperatures high enough to create final abundance distribution composed of primarily carbon and oxygen in their core. After losing their stellar envelopes, these stars are carbon-oxygen white dwarfs. However, if such a star has a companion of sufficient mass, it will eventually explode in a type Ia supernova. Lastly, are stars of mass  $8.0 M_{\odot} \lesssim M$ , which go through sequences of carbon, neon, oxygen, and silicon burning to produce a dominantly iron-nickel core. At this point, as the stars are more massive than the Chandrasekar limit, the gravitational attraction will exceed the support of electron degeneracy pressure causing a core collapse (type II) supernova. Depending on the star's mass at this stage, it will become either a neutron star or black hole. While not the topic of this thesis, such explosive scenarios are currently an area of intense research as they are the location of many unresolved issues of nuclear astrophysics, including what the National Research Council identified in 2003 as one of the eleven greatest unanswered questions of the century, namely the origin of the elements heavier than iron [citeTurner2003](#).

### 1.1.3 Hydrogen Burning

The lifetimes of stars along the main sequence vary drastically, from millions of years to trillions of years, depending on the star's properties when forming. Likewise, the dominant type of hydrogen burning that occurs during the main sequence phase is also highly dependent on stellar characteristics like mass and initial composition. Broadly, there are two sets of nuclear processes

that comprise the hydrogen burning phases in stellar cores, the *pp chains* and the CNO cycles, with each ultimately functions in a similar way, to convert four hydrogen nuclei to one helium nucleus, releasing  $\sim 26$  MeV of energy citeRoflsBook.

The *pp chains* are the main energy generator in smaller stars with core temperatures below 20 MK citeRyanNortonBook, like the sun. There are three variations of the *pp chains* (denoted ppI, ppII, and ppIII), shown below.

<u>ppI</u>	<u>ppII</u>	<u>ppIII</u>
$p(p, e^+ \nu) d$	$p(p, e^+ \nu) d$	$p(p, e^+ \nu) d$
$d(p, \gamma) {}^3\text{He}$	$d(p, \gamma) {}^3\text{He}$	$d(p, \gamma) {}^3\text{He}$
${}^3\text{He}({}^3\text{He}, 2p) {}^4\text{He}$	${}^3\text{He}({}^4\text{He}, \gamma) {}^7\text{Be}$	${}^3\text{He}({}^4\text{He}, \gamma) {}^7\text{Be}$
	${}^7\text{Be}(e^- \nu) {}^7\text{Li}$	${}^7\text{Be}(p, \gamma) {}^8\text{B}$
	${}^7\text{Li}(p, \alpha) {}^4\text{He}$	${}^8\text{B}(e^+ \nu) {}^8\text{Be}$
		${}^8\text{Be}(\alpha) {}^4\text{He}$

Between the three branches there are clear similarities and differences. The energy released between each of ppI, ppII, and ppIII are 26.20 MeV, 25.66 MeV, and 19.75 MeV, respectively, with the difference coming from the amount of energy carried away by the electrons, positrons, and neutrinos. Of these chains, ppI is the most prominent, occurring  $\sim 85$  % of the time, where the remainder branches off as a  ${}^3\text{He}$  nucleus will fuse with a  ${}^4\text{He}$  nucleus, resulting in the ppII or ppIII chain, occurring  $\sim 14.99$  % and  $\sim 0.1$  % of the time, respectively citeRyanNortonBook. Regardless of the branching for the *pp chains*, each starts with the  $p(p, e^+ \nu) d$  reaction. This reaction is governed purely by the weak interaction, and thus is about 20 orders of magnitude slower than those proceeding via the strong interaction citeRoflsBook, like the reactions in the chains that follow. Therefore, energy production, nucleosynthesis, and stellar evolution timescales for stars dominated by the *pp chains* are restricted by the  $p(p, e^+ \nu) d$  reaction.

However, for most stars the CNO cycles are the dominant energy source. Stellar energy generation depends sensitively on the temperature in the star's core, which is closely tied to its mass. For stars of mass  $M \gtrsim M_\odot$ , where cores contain carbon and oxygen seed nuclei and temperatures exceed 20 MK, the CNO cycles' energy production overtakes that of the *pp chains*. Thus, the knowledge of the overall rate of this cycle is important for the study of their evolution.

The CNO cycles are the collection of four similar energy producing cycles broadly characterized by their synthesis of helium from hydrogen with a carbon catalyst, seeded by earlier generations of stars. There are four CNO cycles, listed below with their relationships shown in Fig. ??.

<u>CNO1</u>	<u>CNO2</u>	<u>CNO3</u>	<u>CNO4</u>
$^{12}\text{C} (p, \gamma) ^{13}\text{N}$	$^{14}\text{N} (p, \gamma) ^{15}\text{O}$	$^{15}\text{N} (p, \gamma) ^{16}\text{O}$	$^{16}\text{O} (p, \gamma) ^{17}\text{F}$
$^{13}\text{N} (\beta^+ \nu) ^{13}\text{C}$	$^{15}\text{O} (\beta^+ \nu) ^{15}\text{N}$	$^{16}\text{O} (p, \gamma) ^{17}\text{F}$	$^{17}\text{F} (\beta^+ \nu) ^{17}\text{O}$
$^{13}\text{C} (p, \gamma) ^{14}\text{N}$	$^{15}\text{N} (p, \gamma) ^{16}\text{O}$	$^{17}\text{F} (\beta^+ \nu) ^{17}\text{O}$	$^{17}\text{O} (p, \gamma) ^{18}\text{F}$
$^{14}\text{N} (p, \gamma) ^{15}\text{O}$	$^{16}\text{O} (p, \gamma) ^{17}\text{F}$	$^{17}\text{O} (p, \gamma) ^{18}\text{F}$	$^{18}\text{F} (\beta^+ \nu) ^{18}\text{O}$
$^{15}\text{O} (\beta^+ \nu) ^{15}\text{N}$	$^{17}\text{F} (\beta^+ \nu) ^{17}\text{O}$	$^{18}\text{F} (\beta^+ \nu) ^{18}\text{O}$	$^{18}\text{O} (p, \gamma) ^{19}\text{F}$
$^{15}\text{N} (p, \alpha) ^{12}\text{C}$	$^{17}\text{O} (p, \alpha) ^{14}\text{N}$	$^{18}\text{O} (p, \alpha) ^{15}\text{N}$	$^{19}\text{F} (p, \alpha) ^{16}\text{O}$

As with the *pp chains*, the net result of each of the CNO cycles is the conversion of four protons into helium, releasing  $\sim 26$  MeV of energy in the process citeRyanNortonBook. Additionally, all of the heavier elements (carbon, nitrogen, oxygen, and fluorine) are only catalysts, with their overall abundance unchanged through the cycles while only the hydrogen is consumed. Therefore, this implies that the CNO cycles can occur even if the amount of heavy elements is relatively small, in the case of only being seeded by a single prior generation of stars citelliadisBook. Of the cycles, however, the main CNO1 cycle contributes  $\sim 99\%$  of the CNO energy production citeAdelberger1998, so hereafter CNO1 will be referred to as simply the CNO cycle, while the others will be designated as needed.

Within the CNO cycle, the  $^{14}\text{N} (p, \gamma) ^{15}\text{O}$  reaction is the slowest and thus the rate-limiting step of the whole process, ruling the energy production and the overall time spent in this burning phase, evidenced recently by the adjustment of the estimation of globular cluster ages citeImbriani2004.

The relative energy production between the *pp chains* and CNO cycles are shown in Fig. ?. It can be seen that the CNO cycle accounts for  $<1\%$  of solar energy production citeAdelberger1998, Adelberger2011. However, it produces  $1.6\%$  of solar neutrinos through the  $\beta$ -decay of  $^{13}\text{N}$  and  $^{15}\text{O}$  citeBahcall2004, which can be used to test assumptions of the Standard Solar Model (SSM), as these rates are one of the largest sources of uncertainty in model predictions citeSerenelli2013. Efforts to measure the neutrino fluxes from the  $\beta$ -decays of  $^{13}\text{N}$  and  $^{15}\text{O}$  are either ongoing or planned at the Borexino, Super-Kamiokande, and SNO+ laboratories citeJose2011.



These laboratories are well known for their contributions in solving the *solar neutrino problem* citeJose2011 (and references therein). However, after this solar problem was solved, a new problem arose, named the solar abundance problem citeAdelberger2011, Pena-Garay2008, Serenelli2009. The problem is as follows, solar models describe the structure, composition, and evolution of a  $1M_{\odot}$  star from ignition through the sun's current age and are constrained by the plethora of helioseismology data from the Sun. Recent analyses of the Sun's photosphere lead to a reduced metallicity estimate, destroying the agreement between helioseismology and solar models citeAsplund2005, Basu1997. In discussing potential solutions to this problem, it was proposed to use the neutrino fluxes from the  $\beta$ -decay of CNO isotopes  $^{13}\text{N}$  and  $^{15}\text{N}$  to address this problem, as these quantities depend linearly on their abundance within the solar core citeHaxton2008. Therefore, with the measurement of these neutrino fluxes imminent, it is ever more important to have precise knowledge of the relevant nuclear cross-sections.

Due to the importance of the  $^{14}\text{N}(p,\gamma)^{15}\text{O}$  reaction, it is the focus of this work. Presented first, in Sec. ?? and Sec. 1.4, are an overview of nuclear reaction theory and  $R$ -matrix formalism. The current state of knowledge surrounding the reaction, its uncertainties, and previous measurements are discussed in Sec. 1.5. After which, a summary of the Doppler Shift Attenuation Method for measuring extremely short nuclear lifetimes will be given in Sec. 1.6. An outline of the remainder of this work will finally be presented in Sec. 1.7.

## 1.2 Thermonuclear reaction rates

Stars are fueled by the energy released during nuclear reactions. Recall that a nuclear reaction can be written as

$$a + A \rightarrow b + B + Q \quad \text{or} \quad A(a,b)B^* \quad (1.1)$$

where  $a$  denotes the projectile,  $A$  the target nucleus,  $b$  the ejectile,  $B$  the reaction product, and  $Q$  the energy released (or absorbed) during the reaction, typically present as kinetic energy distributed among the reaction products. For this reaction to occur, the initial nuclei must have enough energy to overcome the Coulomb repulsion created by their constituent protons. The probability of their interaction, called their cross section ( $\sigma$ ), is therefore energy dependent. As stars are powered by

thousands of such reactions at a variety of energies, the understanding of nuclear cross-sections are crucial components to the subsequent understanding of stellar evolution and nucleosynthesis.

Consider a stellar environment filled with two types of nuclei with number densities (nuclei /  $\text{cm}^3$ )  $N_1$  and  $N_2$ , respectively, and relative velocity  $v$ . The rate of reaction for these two species per unit volume would then be proportional to the probability that a given pair of particles would react multiplied by the number of pairs that interact per unit time. Mathematically, the reaction rate  $R_{12}$  would therefore be

$$R_{12} = \frac{N_1 N_2}{1 + \delta_{12}} v \sigma(v) \quad (1.2)$$

with  $\delta_{12}$  to prevent overcounting if the particles are identical. In stellar environments, the relative velocity between the two particles can take a range of values related to the temperature,  $T$ . The probability distribution of the potential relative velocities,  $P(v)$ , is described by the Maxwell-Boltzmann distribution citeRyanNortonBook:

$$P(v) = 4\pi v^2 \left( \frac{\mu}{2\pi kT} \right)^{3/2} \exp \left( -\frac{\mu v^2}{2kT} \right) \quad (1.3)$$

where  $k$  is the Boltzmann constant, relating the kinetic energy of a particle to the temperature of its environment, and  $\mu = m_1 m_2 / (m_1 + m_2)$  is the reduced mass of the two nuclei. Explicitly, the probability that a given pair of nuclei having a relative velocity between  $v$  and  $v + dv$  is  $P(v)dv$  and satisfies the unity expression

$$\int_0^\infty P(v) dv = 1. \quad (1.4)$$

Therefore, the reaction rate per particle pair  $\langle \sigma v \rangle$  with relative velocity  $v$  is the average value of  $v$  multiplied with  $\sigma(v)$  for a given temperature,

$$\langle \sigma v \rangle = \int_0^\infty v P(v) \sigma(v) dv. \quad (1.5)$$

Using a few useful substitutions, this formulation allows us to rewrite Equation 1.2, the general reaction rate, as a function of energy instead of velocity. To do this, recall that the kinetic energy is  $E = \frac{1}{2} \mu v^2$  and its derivative is  $dE/dv = \mu v$ . By explicitly writing the Maxwell-Boltzmann distribution into and replacing the appropriate terms in Equation 1.5 leads to

Figure 1.1. Schematic plot of the combined attractive nuclear and repulsive Coulomb potentials.

$$\langle \sigma v \rangle = \left( \frac{8}{\pi \mu} \right)^{1/2} \left( \frac{1}{kT} \right)^{3/2} \int_0^\infty \sigma(E) E \exp \left( -\frac{E}{kT} \right) dE. \quad (1.6)$$

It is important to note that the only unknown in the entirety of the reaction rate is the expression of the nuclear cross section as a function of energy,  $\sigma(E)$ . Therefore, to understand the reaction rates for stellar environments,  $\sigma(E)$  needs to be determined.

Recall that earlier, the cross section,  $\sigma(E)$ , is the probability of two nuclei reacting if brought together at a specific energy,  $E$ . While this quantity is an expression of the probability of reaction, it is analogous to the classical, cross-sectional area of the nucleus, so it is expressed in units of area (specifically barns, where  $1 \text{ b} = 10^{-24} \text{ cm}^2$ ). An insightful description is to think of the cross section coming from throwing two balls at each other with random perturbations off of a common axis, classically. If either ball's size changes (cross-sectional area), the chances of hitting will also change in a manner that is directly proportional to the alteration of the respective sizes of the balls since the total cross-sectional area is  $\sigma = \pi(R_1 + R_2)^2$ . For our quantum mechanical nuclei, the nuclear size needs to be replaced with the deBroglie wavelength, resulting in  $\sigma = \pi\lambda$ . Translating this into another formulation that is more familiar, the cross section is the number of reactions occurring divided by the number of potential reactions, given as

$$\sigma = \frac{N_R}{(N_i N_t)/A}, \quad (1.7)$$

where  $N_R$  is the number of reactions that take place per unit time,  $N_i$  is the number of incident nuclei per unit time,  $N_t$  is the number of target nuclei within the area of incidence,  $A$ .

In astrophysical environments, nuclei typically do not have enough energy to overcome the Coulomb repulsion provided by the protons within the nucleus and combine with the attractive nuclear strong force. A diagram of the combined nuclear and Coulomb potentials is given in Fig. ???. The repulsive Coulomb interaction causes the cross section to drop quickly at low center-of-mass energies citelliadisBook. Thus, for such reactions to occur, nuclei must actually tunnel through the Coulomb barrier.

The Coulomb penetrability,  $P$ , can be approximated as the leading term of the  $s$ -wave ( $\ell = 0$ )

Figure 1.2. The energy dependence of the nuclear cross section and astrophysical S-factor

barrier transmission coefficient:

$$P = \exp(-2\pi\eta), \quad (1.8)$$

where  $\eta$  is the Sommerfeld parameter,

$$\eta = \frac{Z_1 Z_2 e^2}{4\pi\epsilon_0 \hbar v} = \alpha Z_1 Z_2 \sqrt{\frac{\mu c^2}{2E_{cm}}}, \quad (1.9)$$

where  $Z_i$  is the respective proton number of each nucleus,  $v$  is the incident center-of-mass velocity,  $\alpha \approx 1/137$  is the fine-structure constant,  $\mu$  is the reduced mass of the system, and  $E_{cm}$  is the center of mass energy of the interacting nuclei. Numerically, it is convenient to evaluate the quantity  $2\pi\eta$ , known as the Gamow factor, as

$$2\pi\eta = 0.989534 Z_1 Z_2 \left( \frac{\mu}{E_{cm}} \right)^{1/2}, \quad (1.10)$$

where  $E_{cm}$  is expressed in units of MeV and  $\mu$  in atomic mass units (amu or simply, u).

By factoring the Coulomb penetrability out of the cross section, we can separate the contributions from the Coulomb barrier to isolate the nuclear physics in the astrophysical  $S$ -factor,  $S(E)$ ,

$$\sigma(E) = \frac{1}{E} S(E) e^{-2\pi\eta}. \quad (1.11)$$

The astrophysical  $S$ -factor is slowly varying with energy, unlike the nuclear cross section. Fig. ?? provides a comparison of the energy dependence of both the cross section and  $S$ -factor, where you can see that the cross section drops by orders of magnitude in an energy regime where the  $S$ -factor is relatively constant. This implies that the Coulomb effects can obscure important nuclear physics effects. Additionally, as the  $S$ -factor is slowly varying, extrapolations of it's behavior towards zero energy from higher energy data are significantly more reliable than those made from cross section data.

Now, after defining the  $S$ -factor, the reaction rate can be written finally as

$$\langle \sigma v \rangle = \left( \frac{8}{\pi\mu} \right)^{1/2} \left( \frac{1}{kT} \right)^{3/2} \int_0^\infty S(E) \exp \left( -\frac{E}{kT} - \frac{b}{E^{1/2}} \right) dE. \quad (1.12)$$

Figure 1.3. The two dominant terms of the reaction rate calculation and their convolution (Gamow peak).

where  $b$  has units of  $(\text{MeV})^{1/2}$  and is given as

$$b = 0.989534 Z_1 Z_2 \mu^{1/2}. \quad (1.13)$$

Recall that one of the most useful features of  $S(E)$  is that it is typically smoothly varying with respect to energy, meaning that the reaction rate in total is dependent primarily on the exponential term inside the integrand of Eq. 1.12. The two components of this term arise from the Coulomb penetrability and the Maxwell-Boltzmann velocity distribution described in Eq. 1.3. The convolution of these two quantities can be used to estimate the energy range where the reaction rate should be maximized for given stellar temperatures [citeIliadisBook](#).

The Coulomb penetrability and Maxwell-Boltzmann velocity distribution have opposite behaviors in energy regimes with the penetrability dropping to zero at low energies while the probability distribution for the velocities is maximized at low energies and vice-versa at high energies. The product of the terms is therefore negligible for nearly all energies. However, for a small set of energies this product, and therefore the reaction rate, maximizes. This behavior, as well as their product, commonly called the Gamow Peak, is presented in Fig. ??.

The Gamow peak's maximum can be obtained with basic calculus on the exponential term in Eq. 1.12 by setting the derivative with respect to energy equal to zero and solving for the energy value. This results in the maximum energy of the reaction rate being

$$E_0 = \left( \frac{bkT}{2} \right)^{2/3}. \quad (1.14)$$

For a given stellar temperature,  $T$ , the average effective energy at which the reaction occurs is  $E_0$ . Additionally, this also allows for an approximation of the range of energies over which the reaction primarily occurs, provided that the  $S$ -factor is smoothly varying (which is not true if resonances are present, which will be discussed in the next section). This range of energies is known as the Gamow Window,  $\Delta$ :

$$\Delta = \frac{4}{\sqrt{3}} \sqrt{E_0 kT}. \quad (1.15)$$

The Gamow window identifies the range of energies over which experimental data should be taken to provide a complete understanding of stellar processes. As an example, the  $^{14}\text{N}(p, \gamma)^{15}\text{O}$  reaction in the sun has a Gamow peak energy at  $E_0 = 26.6$  keV and  $\Delta = 13.6$  keV, meaning that measuring the cross section in the energy range of 19.8 - 33.4 keV is crucial in the understanding of this reaction.

Unfortunately, though, measuring at energies this low is not feasible, experimentally. This is because at these energies the signal-to-noise ratio of observables drops dramatically and the signals of interest are obscured within background noise. To provide accurate measurements of such situations, experiments must necessarily then occur in the timescale of years to measure a single datum. This is simply unfeasible, practically, and our understanding must rely on extrapolations from higher-energy data. As the  $^{14}\text{N}(p, \gamma)^{15}\text{O}$  reaction is not alone in having a Gamow window at such low energies, extrapolation techniques must be employed to describe the cross section and  $S$ -factor for nearly all astrophysically important reactions at the Gamow window.

### 1.3 Nuclear reactions

For the  $^{14}\text{N}(p, \gamma)^{15}\text{O}$  reaction, both resonant and direct capture contributions are important. Resonant reactions are those in which an incoming particle combines with a target to form an excited state in a compound nucleus and then subsequently decay as part of a two-step process. Alternatively, direct capture reactions are those in which the particle pair proceeds directly to a final, bound nuclear state in one step. An energy level diagram of the  $^{14}\text{N}(p, \gamma)^{15}\text{O}$  reaction is shown in Fig. ??.

#### 1.3.1 Direct capture reactions

The other side of the proverbial coin from resonant reactions is direct capture, or nonresonant reactions. Such cases are defined as those in which the cross section and  $S$ -factor vary smoothly with energy, being the result of a one-step, electromagnetic process where the capture proceeds from the initial state of two incident particles to the final, bound state of the system. This process is

Figure 1.4. An energy level diagram of the  $^{14}\text{N}(p, \gamma)^{15}\text{O}$  reaction. This shows the pathways of decay to the ground state of the  $^{15}\text{O}$  nucleus. The paths shown in red indicate a resonance reaction, with the formation of the compound nucleus in an excited state, while the path in blue shows a direct capture process, proceeding immediately to the ground state.

also highlighted as a part of Fig. ??.

With nonresonant reactions, the  $S$ -factor varies smoothly with energy. This means that the earlier characterization of the  $S$ -factor, reaction rate, and Gamow energy/window parameters in Equations 1.6 - 1.15 are applicable for the case of direct reactions. In extrapolating experimental data to stellar energy ranges, it is often useful to express an effective  $S$ -factor,  $S_{\text{eff}}$  from the Taylor expansion of the component functions citelliadisBook,

$$S_{\text{eff}} = S(0) \left(1 + \frac{5kT}{36E_0}\right) + S'(0)E_0 \left(1 + \frac{35kT}{36E_0}\right) + \frac{1}{2}S''(0)E_0^2 \left(1 + \frac{89kT}{36E_0}\right), \quad (1.16)$$

where  $E_0$  is the Gamow peak energy from Equation 1.14. Armed with this expansion, the  $S$ -factor can be successfully extrapolated to low, stellar energies in cases where the  $S$ -factor varies slowly with energy. This means that for nonresonant reactions,  $S(E)$  can be approximated by its zero-energy value,  $S(0)$ , and only small corrections given by its first and second derivatives,  $S'(0)$  and  $S''(0)$ , respectively.

### 1.3.2 Resonant reactions

The presence of a resonance enhances the cross section at its specific center-of-mass energy and means that the  $S$ -factor no longer varies smoothly with respect to energy. The specific increase is highly dependent on the situation since, as a two-step process, it depends on the probability of both forming the compound nucleus and decaying via a specific pathway, also shown in Fig. ?. To understand this mathematically, consider an isolated, narrow resonance at energy  $E_R$ ; the reaction cross section under the influence of such a resonance is described by the Breit-Wigner formula:

$$\sigma_{BW}(E) = \pi\lambda^2 \frac{2J_R + 1}{(2J_1 + 1)(2J_2 + 1)} \frac{\Gamma_{\text{in}}\Gamma_{\text{out}}}{(E - E_R)^2 + \Gamma_T^2/4} \quad (1.17)$$

where  $\lambda$  is the deBroglie wavelength corresponding to the incident momentum,  $p = \hbar/\lambda$ ,  $J_1$  and  $J_2$  are the spins of the target and projectile,  $J_R$  is the spin of the resonance in the compound nucleus,  $\Gamma_{\text{in}}$  and  $\Gamma_{\text{out}}$  are the entrance and exit reaction channel widths (essentially the probability for a particular part of the process to occur), and  $\Gamma_T$  is the total width ( $\Gamma_t = \Gamma_1 + \Gamma_2 + \dots \Gamma_n$ ). The total width is related to the mean lifetime,  $\tau$ , of the excited state by

$$\Gamma_T\tau = \hbar. \quad (1.18)$$

For most nuclear states, the widths can be determined experimentally, allowing for the under-

standing of the total width,  $\Gamma_T$ . However, due to many of the earlier described constraints, this is not always easy in practice. Additionally, the fact that different resonances have different strengths and can potentially dominate the contributions of others adds another complication. On the other hand, this implies that the total width will be dominated by that specific decay's width. If the dominant decay is one of the primary entrance or exit channels astrophysically, this will have a proportionally large effect on the overall cross section and reaction rate. In the case of the  $^{14}\text{N}(p, \gamma)^{15}\text{O}$  reaction, there are two states near the proton threshold, one above and one below in energy, as shown in Fig. ??, and these two provide the largest contributions to the overall astrophysical reaction rate.

To characterize this, we replace the Breit-Wigner formula from Equation 1.17 into the reaction rate equation 1.6 citeIliadisBook. This leads to

$$\langle \sigma v \rangle_{\text{BW}} = \left( \frac{8}{\pi \mu} \right)^{1/2} \left( \frac{1}{kT} \right)^{3/2} \int_0^\infty \sigma_{\text{BW}}(E) E \exp \left( -\frac{E}{kT} \right) dE. \quad (1.19)$$

Because we are considering a narrow energy range for this resonance, both the energy,  $E$ , and the exponential term provided by the Maxwell-Boltzmann velocity distribution,  $\exp(-E/kT)$ , are constant over the integration. This allows us to rewrite the integral as

$$\langle \sigma v \rangle_{\text{BW}} = \left( \frac{8}{\pi \mu} \right)^{1/2} \left( \frac{1}{kT} \right)^{3/2} E_R \exp \left( -\frac{E_R}{kT} \right) \int_0^\infty \sigma_{\text{BW}}(E) dE. \quad (1.20)$$

The previous integral is proportional to the area under the resonance cross section and is known as the resonance strength. By substituting the Breit-Wigner formula, the integral becomes

$$\int_0^\infty \sigma_{\text{BW}}(E) dE = \pi \lambda_R^2 \left( \frac{2J_R + 1}{(2J_1 + 1)(2J_2 + 1)} \right) (1 + \delta_{12}) \Gamma_{\text{in}} \Gamma_{\text{out}} \int_0^\infty \frac{1}{(E - E_R)^2 + (\Gamma_T/2)^2} dE, \quad (1.21)$$

which is solved analytically as

$$\int_0^\infty \sigma_{\text{BW}}(E) dE = \pi \lambda_R^2 \left( \frac{2J_R + 1}{(2J_1 + 1)(2J_2 + 1)} \right) (1 + \delta_{12}) \frac{\Gamma_{\text{in}} \Gamma_{\text{out}}}{\Gamma_T}. \quad (1.22)$$

For simplicity, the statistical factor,  $\omega$ , is now defined as

$$\omega = \frac{2J_R + 1}{(2J_1 + 1)(2J_2 + 1)} (1 + \delta_{12}) \quad (1.23)$$

and the width ratio,  $\gamma$ , is



$$\gamma = \frac{\Gamma_{\text{in}}\Gamma_{\text{out}}}{\Gamma_T}, \quad (1.24)$$

leading to

$$\int_0^\infty \sigma_{\text{BW}}(E)dE = 2\pi^2 \lambda_R^2 \omega \gamma. \quad (1.25)$$

The product  $\omega\gamma$  is called the resonance strength and is very important for reaction rate calculation, since the rate is dependent primarily on it and the resonance energy,  $E_R$ . This can be seen by implementing this integral calculation with the earlier derivation in Equation 1.19, resulting in

$$\langle \sigma v \rangle = \left( \frac{2\pi}{\mu kT} \right)^{3/2} (\omega\gamma) \hbar^2 \exp\left(-\frac{E_R}{kT}\right). \quad (1.26)$$

#### 1.4 $R$ -matrix theory

In many cases, the nuclear cross-section landscape is quite complicated, with the combined effects of multiple resonances and direct capture contributions. With all of this overlap, the Breit-Wigner formulation starting in Equation 1.17 is no longer valid. Therefore, a reliable theory accounting for all contributions and interferences is needed to describe relevant information and perform meaningful extrapolations. For these purposes,  $R$ -matrix theory was developed and is now commonly used in nuclear astrophysics calculations; details of its formal derivation can be found in References citeLane1958, Azuma2010.

The core concept of  $R$ -matrix theory is to describe the wave function of the system by matching individual components in the region of the compound nucleus where the nuclear potential present to an exterior region in which only the Coulomb potential contributes and nucleons are treated as individual particles. At the boundary of these two regions, also known as the channel radius  $a_c$ , the wave functions and their derivatives must match. The  $R$ -matrix actually relates these wave functions for each different reaction channel and is defined as

$$\mathbf{R}_{c'c} = \sum_{\lambda} \frac{\gamma_{\lambda c'} \gamma_{\lambda c}}{E_{\lambda} - E}, \quad (1.27)$$

where  $c$  and  $c'$  are the respective entrance and exit channels of the given reaction and the  $\gamma_{\lambda}$  is the reduced width, given as

$$\gamma_{\lambda}^2 = \hbar^2 / (2ma_c) u_{\lambda}^2(a_c), \quad (1.28)$$

with the  $u_\lambda$  forming a complete set of basis states that satisfy the Schrödinger equation.

While the theory is named for the  $R$ -matrix, the cross section is actually calculated through other intermediate quantities, namely the collision matrix,  $\mathbf{U}$ , and the transition matrix,  $\mathbf{T}$ . The collision matrix relates specifically the incoming channels,  $y_c$ , to those of the outgoing particles,  $x_c$ , defined as

$$x_c = - \sum_{c'} \mathbf{U}_{c'c} y_{c'}. \quad (1.29)$$

Ultimately,  $\mathbf{U}$  is proportional to the  $R$ -matrix as

$$\mathbf{U} \propto |\mathbf{R}|^2. \quad (1.30)$$

The transition matrix, on the other hand, is defined through the collision matrix as

$$\mathbf{T}_{c'c} = e^{2i\omega_c} \delta_{c'c} - \mathbf{U}_{c'c}, \quad (1.31)$$

, where  $\omega_c$  represents the Coulomb phase shift and  $\delta_{c'c}$  is the Dirac delta function relating channels  $c'$  and  $c$ . The angle integrated cross section is then

$$\sigma_{\alpha'\alpha} = \frac{\pi}{k_\alpha^2} \sum_{J\ell'\ell s's} \omega |\mathbf{T}_{c'c}^J|^2 \quad (1.32)$$

where the  $\alpha$ 's identify the interacting particle pair, the  $\ell$ 's are the respective orbital angular momenta of the particles, the  $s$ 's are their respective spins,  $J$  is the total angular momentum of the system, and  $\omega$  is the statistical spin factor as defined by Equation 1.23.

In this work, the multichannel, multilevel  $R$ -matrix code AZURE [citeAzuma2010](#) was used to perform the calculations. A user inputs the spin-parity of the nuclear states, initial energies, partial widths of the excited states, the ANCs of bound states, and any external cross section or  $S$ -factor data into AZURE. The computation of  $S$ -factor and cross section are done via a simple GUI interface. The results are truncated to finite eigenstates behind the scenes to allow the code to operate quickly. As such, a background pole is typically included at high-energy to account for contributions from states not included in the calculations. The theory is also referred to as phenomenological  $R$ -matrix because each of the  $\gamma_\lambda$ 's and  $E_\lambda$ 's in Equation 1.27 are free fit parameters.

## 1.5 The $^{14}\text{N}(p,\gamma)^{15}\text{O}$ reaction

The  $^{14}\text{N}(p,\gamma)^{15}\text{O}$  reaction has been investigated many times in recent years by a wave of campaigns spurred by new facilities, equipment, and analyses citeSchroeder1987, Bertone2001, Bertone2002, Formicola2004, Yamada2004, Imbriani2004, Imbriani2005, Runkle2005, Bemmerer2006, Lemut2006, Schurmann2008, Marta2008, Marta2010, Marta2011a, Marta2011b, Michelagnoli2013, Galinski2014, Szucs2015, Daigle2016, Li2016, Wagner2017. Collectively, these experiments represent an effort to understand the astrophysical  $S$ -factor at stellar energies through both direct and indirect methods. The indirect approaches have two faces: measuring the width of the subthreshold state at excitation energy  $E_x = 6792$  keV ( $E_R = -505$  keV) and the Asymptotic Normalization Coefficient (ANC) of the ground state, while the direct approach is simply that - measuring the cross section to low energies and extrapolating from that data to astrophysical energies.

### 1.5.1 Reaction cross-section

- History of measurement (lots of citations)
- R-matrix reanalysis
- LUNA
- TUNL
- Qian -¿ primary errors left

### 1.5.2 Lifetime

- Existing literature
- Indirect method
- inverse vs. forward kinematics
- Isobaric analog state

## 1.6 The Doppler Shift Attenuation Method for lifetime measurements

### 1.7 Thesis outline

In this dissertation, the results of a series of experiments and subsequent analyses performed to better understand the low energy behavior of the  $^{14}\text{N}(p,\gamma)^{15}\text{O}$  will be presented. These include the measurement of the  $^{14}\text{N}(p,\gamma)^{15}\text{O}$  reaction at the University of Notre Dame Nuclear Science Laboratory (NSL) and the Compact Accelerator System for Performing Astrophysical Research

(CASPAR), located in the Sanford Underground Research Facility in the renovated Homestake Gold Mine in South Dakota, as well as a direct measurement of the lifetime of the 6.79 MeV level in  $^{15}\text{O}$ .

An outline of the experimental techniques used in these measurements will be presented in Chapter 2. There will be a brief overview of the equipment common to each of the measurements, with emphasis on the Van de Graaff accelerators and High-purity Germanium detectors used. Following this, the specific features of the different types of measurements and the facilities in which they were made will be presented.

Chapters 3 - 5 will present details on the different facets of the data reduction and analysis. The first of these, Chapter 3, presents the data for  $^{14}\text{N}(p, \gamma)^{15}\text{O}$  taken at the NSL and CASPAR while detailing the process by which the cross-section and astrophysical  $S$ -factor were extracted. Shifting focus, Chapter 4 will focus on the Monte Carlo code that was developed and used to simulate the lifetime of the states in  $^{15}\text{O}$ , presenting the results of these tests and displaying their ability to reproduce experimental cases. Finally, Chapter 5 will present the actual lineshape analysis of the data done to extract the lifetime of the 6.79 MeV state in  $^{15}\text{O}$ . The validity of the method will be checked against other known levels populated in the reaction.

The cross-section information and newly measured lifetime will be utilized in a new  $R$ -matrix analysis of the  $^{14}\text{N}(p, \gamma)^{15}\text{O}$  reaction, presented in Chapter 6. The new constraints these data provide on the low-energy behavior of the extrapolated  $S$ -factor will be provided, alongside a description of their impact to relevant astrophysical quantities.

Finally, the contents of this dissertation will be summarized in Chapter 7. This will present an overview of the described measurements, analysis, respective impacts, and future outlook.

## CHAPTER 2

### EXPERIMENTAL SETUP AND PROCEDURES

#### 2.1 Introduction

This set of data was taken over the course of five\* separate experiments. The first occurred at the University of Notre Dame's Nuclear Science Laboratory (NSL) in January of 2018 and covered the proton energy range of  $E_p = 800 - 1200$  keV. The experiment was then continued at the Compact Accelerator System for Performing Nuclear Astrophysics (CASPAR) facility at the Sanford Underground Research Facility located in Lead, South Dakota in three increments: February 2018, May 2018, and August / September 2018. These measurements covered the energy range from  $E_p = 270 - 1200$  keV, in order to measure the  $^{14}\text{N}(p, \gamma)^{15}\text{O}$  reaction cross-section to compare the performance of the CASPAR facility to an above-ground laboratory. Finally, in MONTH TIME DATE THING, the final experiment was completed at the NSL, focusing on obtaining the lifetime of the 6793 keV state in  $^{15}\text{O}$ .

#### 2.2 Accelerators, beamline, and high-purity Germanium detectors

##### 2.2.1 Van de Graaff accelerators

##### 2.2.2 Ion sources

##### 2.2.3 Beamline

#### 2.3 High-purity Germanium detectors

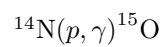
#### 2.4 Cross-section measurements

#### 2.5 Lifetime measurement

## CHAPTER 3

### CROSS SECTION DATA REDUCTION AND ANALYSIS

#### 3.1 Introduction



#### 3.2 Energy calibration

#### 3.3 Efficiency

##### 3.3.1 Total efficiency

##### 3.3.2 Full energy peak efficiency

#### 3.4 Summing corrections

#### 3.5 Target characterization

#### 3.6 Cross-section determination

## CHAPTER 4

### MONTE CARLO SIMULATIONS FOR LIFETIME MEASUREMENTS WITH DSAM

4.1 Simulations with the Geant4 package

4.2 Determining a nuclear lifetime

## CHAPTER 5

### THE LIFETIME OF THE 6.79 MEV STATE IN $^{15}\text{O}$

#### 5.1 Data analysis

##### 5.1.1 Lifetime of **ANOTHER STATE**, 6.17 MeV maybe

##### 5.1.2 Lifetime of the 6.79 MeV state in $^{15}\text{O}$



## CHAPTER 6

### R-MATRIX ANALYSIS

6.1 Fits to the capture data

6.2 Inclusion of the new lifetime

## CHAPTER 7

### RESULTS AND CONCLUSIONS

## APPENDIX A

### GNU GENERALISMS

#### A.1 Definitions

Several definitions are presented in Table A.1 to show both how to do rotated, line-spanning tables, as well as to define some commonly used Gnu terms.

TABLE A.1

## COMMONLY USED Gnu TERMS

Term	Definition
Gnu	Small furry animal that is related to the squirrel (although they won't admit it).
LoG	Abbreviation for the "Leader of Gnus". See Chapter ??.
Twizzlers	Red, twisty candy that is among the most favorite of Gnu foods. Gnus frequently appear overly cute and friendly to humans bearing twizzler packages. This is known as "trolling for twizzlers" among the Gnus.

Finally, Table A.2 shows the top ten Gnus from Table ?? ranked in order by their aggregate score (along with some of the raters' comments). This follows a long-standing Gnu tradition of self-improvement through public announcement of score (which some associate with military origins [? ]). Indeed, this very table has been observed in the Gnu lodge where it was posted for peer review [? ].

Table A.2: Top Ten Gnus From Table ?? With Reviewer Comments. Gnus are Listed Below in Alphabetic Order.

Candidate	Aggregate score	Reviewer Comments
George	7.6	George is an excellent candidate for the LoG. Slightly low C, but hopefully, this 7.6 will be high enough!
Glen	7.2	A little weak on AM and Fr, but good scores overall. One or two more years of experience should be enough.
Goldie	7.0	Dismal score in Fr; suspect it had something to do with strenuous weight loss program this past year.
Gillian	6.9	Excellent C, but a little shabby on the Fu. Suggest more roughage.
Gibby	6.9	Reasonable scores, but need to work on Fr. Gibby is definitely not a morning Gnu.
Genaveve	6.5	Very low Fr; perhaps more coffee? Suggest practicing “cute faces” in the mirror several hours per day.
Giovani	6.2	Very low Fr; suspect hanging out with Genaveve too much.
Gina	6.2	Mediocre Fu, somewhat low AM. Perhaps a future in marketing or advertising?
Garrick	6.2	Fairly low AM. Fu could be better as well; buy a comb. And a mirror. Immediately.
Gardenia	6.0	Dismal AM; very low Fu. Seems to care more about meeting agendas than personal appearance.

## BIBLIOGRAPHY